Structure and band gap tuning of transparent $(Ba_{1-x}Sr_x)SnO_3$ thin films epitaxially grown on MgO substrates

2012 EPL 98 47010

(http://iopscience.iop.org/0295-5075/98/4/47010)

A Letters Journal Exploring the Frontiers of Physics

May 2012

EPL, **98** (2012) 47010
doi: 10.1209/0295-5075/98/47010

www.epljournal.org

Structure and band gap tuning of transparent $(Ba_{1-x}Sr_x)SnO_3$ thin films epitaxially grown on MgO substrates

Qinzhuang Liu[1(a)], Bing Li[1], Jianjun Liu[1], Hong Li[1], Zhongliang Liu[1], Kai Dai[1], Guangping Zhu[1], Peng Zhang[1], Feng Chen[2] and Jianming Dai[2]

[1] *School of Physics and Electronic Information, Huaibei Normal University - Huaibei 235000, PRC*
[2] *Key Laboratory of Materials Physics, Institute of Solid State Physics, and Hefei High Magnetic Field Laboratory, Chinese Academy of Science - Hefei 230031, PRC*

received 14 March 2012; accepted in final form 30 April 2012
published online 30 May 2012

PACS 77.55.Px – Epitaxial and superlattice films
PACS 91.60.Mk – Optical properties
PACS 71.20.-b – Electron density of states and band structure of crystalline solids

Abstract – $(Ba_{1-x}Sr_x)SnO_3$ ($x = 0$–1) (BSSO) films were epitaxially grown on MgO substrates by pulsed laser deposition. X-ray diffraction, atomic force microcopy, and optical transmittance investigations reveal that the lattice and band structure properties of the BSSO films can be modified significantly by changing the Sr content. With increasing Sr content from 0 to 1 in films, the lattice parameters decrease from 4.123 to 4.037 Å gradually, while the optical band gaps energy increases from 3.50 to 4.27 eV linearly, which was attributed to the octahedral tilting distortion pushing up the minimum of conduction band. This large structure and band gap tuning of BSSO films are promising for desired applications in the thin-film architecture.

Alkaline earth stannates with the general formula $RSnO_3$ (R = Ba, Sr and Ca) are important material systems and have attracted much attention in view of their interesting physical properties and perovskite structures similar to the well-understood alkaline earth titanates [1–3]. They have wide applications in thermally stable capacitors, humidity sensors, gas sensors, etc. [2,4,5]. More recently, many substitutions at R and Sn sites have been carried out to modify suitably and further explore the properties of $RSnO_3$ due to their wide band gaps and perovskite structures that are easy to be modulated. For example, La- Sb- and Nd-doped $SrSnO_3$ and $BaSnO_3$ were investigated as promising transparent conductive oxide films [6–8], Mn- and Fe-doped $BaSnO_3$ were found to have room-temperature ferromagnetism [9,10], Sr- and Pb-doped $BaSnO_3$ were proved to have photocatalytic activity [11,12].

Good lattice match and proper energy level alignment with neighboring layers are important characteristics in the design criteria for materials in the thin-film architecture. Among $RSnO_3$, $SrSnO_3$ has a wide band gap of 4.27 eV and a lattice constant $a = 4.032$ Å [13,14], and $BaSnO_3$ behaves as an n-type semiconductor with a wide band gap of 3.4 eV and a lattice constant $a = 4.1163$ Å [15,16]. They were also usually used as insulating buffer layers in the preparation of heterostructures, such as high-critical temperature superconductor $YBa_2Cu_3O_7$ and insulator CeO_2, due to the commensurate lattice [17,18]. However, the solid solutions of stannate Sr-doped $BaSnO_3$ (BSSO) with the tunable crystal lattice and band structure over a relatively wide range through changing the Sr/(Ba,Sr) ratio were rarely studied. Although the photoluminescence and photocatalytic properties of BSSO bulk materials have been reported in the past few years [11,19], from the viewpoint of basic science and application in devices, Sr-doped $BaSnO_3$ in thin-film form are much more attractive and have not been prepared and studied so far. In this letter, we report BSSO epitaxial films with $x = 0$–1 grown on MgO(00l) substrates by the pulsed laser deposition method. The effects of Sr doping on structural and optical properties of the BSSO films were investigated.

The ceramic targets of $(Ba_{1-x}Sr_x)SnO_3$ ($x = 0$, 0.20, 0.40, 0.60, 0.80, 1) were prepared by standard solid reactions [20]. BSSO epitaxial films were deposited on MgO(00l) single crystalline substrates by laser ablation using a 248 nm KrF excimer laser with the repetition rate of 10 Hz and laser energy density irradiated on

(a) E-mail: qzliu@mail.ustc.edu.cn

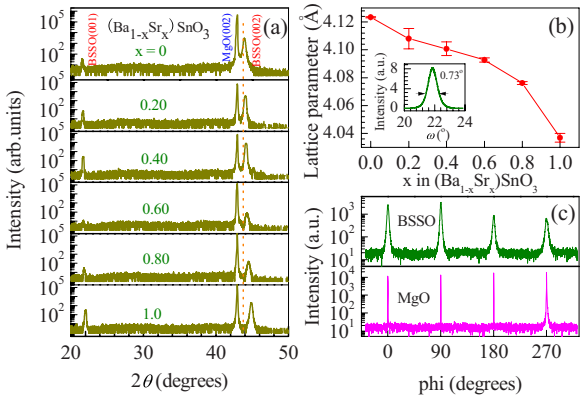

Fig. 1: (Colour on-line) (a) XRD specular linear scans from BSSO/MgO heterostructures at different Sr contents (from $x = 0$ to 1), dashed lines are guides to the eyes. (b) Out-of-plane lattice parameters for BSSO films grown on MgO(00l) substrates as a function of Sr-doping content x, the error bars represent the standard deviation calculated basing on the XRD (00l) peaks position. And the inset shows ω scan rocking curves on the BSSO(002) peak. (c) The Φ scans pattern of both the BSSO films and MgO substrate around(202) reflections.

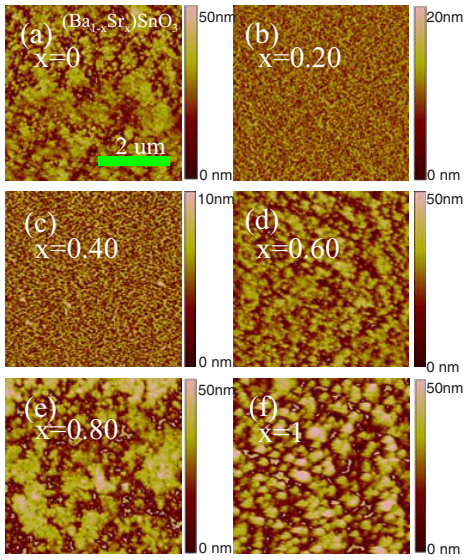

Fig. 2: (Colour on-line) AFM images of BSSO films grown on MgO(00l) substrates with Sr content at (a) $x = 0$, (b) $x = 0.20$, (c) $x = 0.40$, (d) $x = 0.60$, (e) $x = 0.80$, and (f) $x = 1$.

the rotating targets of 1.8 J/cm^2. During deposition the temperature and oxygen pressure were 760 °C and 20 Pa, respectively. Then, the films were *in situ* annealed for 15 min before cooling down in the same oxygen ambient. The film thicknesses were determined to be 380 ± 20 nm by using cross-sectional field-emission scanning electron microscopy, the uncertainty in thickness measurement was estimated to be ±5%. The nominal composition of the films was assumed to be the same as that of the targets. The structures of the films were characterized by X-ray diffraction (XRD) using Cu $K\alpha_1$ radiation with $\lambda = 1.5406$ Å (Philips X'pert). Surface morphologies were observed by using tapping mode atomic force microscopy (AFM, Veeco, Multimode V) with silicon tips (Veeco Nanoprobe Tips RTESP model). The optical transmission and reflection spectra were measured with a conventional spectrophotometer (Hitachi, U-4100).

Figure 1(a) shows the X-ray θ-2θ linear scans from the BSSO/MgO(00l) heterostructures. Only reflections from the (00l) planes of BSSO films and MgO substrates were observed, and no spurious phase or randomly oriented grains appeared in the scans, indicating all the films exhibit preferred orientation along the c-axis. With increasing Sr-doping content from $x = 0$ to 1, the location of the BSSO(00l) reflection peaks shifts towards high-angle direction and then the out-of-plane lattice parameters were obtained from the XRD linear scans with values decreasing gradually from $c = 4.123$ Å of $BaSnO_3$ at $x = 0$ to $c = 4.037$ Å of $SrSnO_3$ at $x = 1$ as shown in fig. 1(b), which are deviated from the linearity as expected by Vegard's law [21]. Similar phenomenon was observed in $Cd_{1-x}Ca_xO$ and $Mg_{1-x}Ni_xO$ systems [22,23]. The decreases in lattice constant are due to the different ionic radii of Ba^{2+} ($R_{ef} = 1.032$ Å) and Sr^{2+} ($R_{ef} = 0.764$ Å) [24]. The full widths at half-maximum of the X-ray rocking curves at (002) peaks were in the range of 0.70°–0.90°, as shown in the inset to fig. 1(b) for BSSO film at $x = 0.4$, which confirm that the films have high crystallinity. In order to check the epitaxial properties, the Φ scans were measured on BSSO(202) and MgO(202) reflections as shown in fig. 1(c), a set of four distinct peaks with 90° separation indicates that the films were coherently grown on MgO(001) substrates.

Figures 2(a)–(f) show the surface morphologies of our BSSO films investigated by AFM with a scanning area $5 \times 5\,\mu$m^2. It was found that the films are uniform and dense without cracks or voids. The root-mean-square surface roughnesses are strongly dependent on Sr content with values of 8.02 ± 0.36, 2.06 ± 0.13, 1.73 ± 0.12, 7.66 ± 0.34, 9.65 ± 0.45, and 12.7 ± 0.74 nm for films at $x = 0$, 0.20, 0.40, 0.60, 0.80, and 1, respectively, the errors were determined by probing on each sample in several regions. At first, the roughnesses decrease with increasing Sr content from pure $BaSnO_3$ and reach a minimum of 1.73 nm in films at $x = 0.40$, showing a very smooth surface. However, on further increasing the Sr content over $x = 0.40$, the roughness begins to increase and at last reach the maximum in films at $x = 1$, namely $SrSnO_3$ films. Meanwhile, the grain sizes become larger with increasing Sr content in films. These results were ascribed to the different effects of the same deposition temperature on film crystallization.

The transmittance and reflection spectra measured in the wavelength range of 200–2000 nm from pure MgO(00l) substrates and BSSO/MgO(00l) heterostructures are shown in fig. 3(a). It can be seen that the obtained films exhibit a high transparency of more than 90% in the visible and near-infrared range, and the

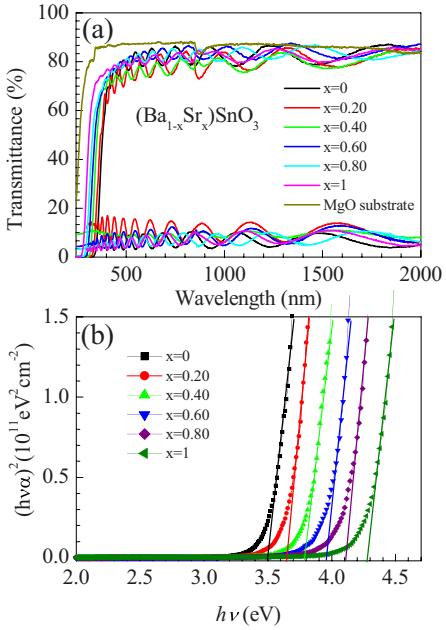

Fig. 3: (Colour on-line) (a) Optical transmission and reflection spectra of pure MgO substrate and the BSSO/MgO heterostructures at different Sr contents. (b) $(h\nu\alpha)^2$ *vs.* $h\nu$ plots of BSSO/MgO(00l) films ($x = 0$, 0.20, 0.40, 0.60, 0.80 and 1).

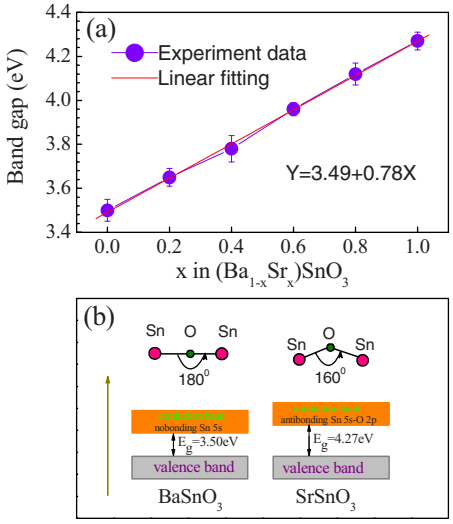

Fig. 4: (Colour on-line) (a) Optical band gaps variation as a function of the Sr content in BSSO films, the error bars originate in the uncertainty in the extrapolation of the absorption curves down to the base line. The solid line is the linear fitting to the experimental data. (b) Electric structures and Sn-O-Sn bond angles for BSSO films at low Sr content $x = 0$ and high Sr content $x = 1$ with band gaps of 3.50 eV and 4.27 eV, respectively.

oscillations of the spectra are due to film interference effect. More interestingly, in the ultraviolet region, the optical absorption edges, corresponding to the band gaps of the BSSO films that are separated by the conduction and valence band edges, shift towards shorter wavelength sides with increasing Sr-doping content in films. For determining the band gaps of the films, the optical absorption coefficients α were calculated using the well-known relation, $\alpha = (1/d)\ln[(1-R)/T]$, where d is the thickness, T is the transmittance, and R is the reflectance of the films. The optical band gap E_g of the BSSO films was determined from the absorption spectra using the equation [25]

$$(h\nu\alpha)^n = A(h\nu - E_g),$$

where A is a constant corresponding to the electron-hole mobility, h is the Planck constant, υ is photon frequency, E_g is the band gap, and n is the exponent that determines the type of electronic transition causing the optical absorption and equals 2, 1/2, 1/3, and 2/3 for direct allowed, indirect allowed, indirect forbidden, and direct forbidden, respectively. $(h\nu\alpha)^2$ were plotted against $h\nu$ in fig. 3(b) and E_g was estimated by extrapolating the linear portion against photon energy. It can be seen that E_g increases continuously from 3.50 to 4.27 eV with increasing Sr-doping content, which is different from the results that the band gaps were in the range from 3.1 to 4.1 eV obtained from optical absorption spectra reported by Mizoguchi *et al.* [19]. For the undoped BSSO films, namely $BaSnO_3$ films, the optical band gap E_g was 3.50 eV, slightly larger than that of 3.40 eV reported by Cerda and Shimizu *et al.* [15,26]. On the other side of Sr-doping at $x = 1$, namely $SrSnO_3$ films, the calculated optical band gap of 4.27 eV is the same as that reported by Endo and Vegas *et al.* [13,14].

Figure 4(a) shows the band gaps of BSSO films, the error bars originate in the uncertainty in the extrapolation of the absorption curves down to the base line. The linear relationship between the band gaps and Sr content x in films was obtained, and it could be fitted by the equation $E_g(x) = 3.49 + 0.78x$ in the entire doping range, where x is the Sr content and $E_g(x)$ corresponds to the band gaps of BSSO films. This phenomenon can be attributed to the effects of octahedral tilting with the increase of Sr content. It is well known that the band gap values of a semiconductor or insulator are dependent on the position and width of the conduction band and valence band. For the pure $BaSnO_3$, it has the ideal cubic perovskite structure with the Sn-O-Sn bond angle of 180°, and the top of the valence band is dominated by the contributions of the O 2p orbitals and the bottom of the conduction band is predominantly composed of nonbonding Sn 5s orbitals [27]. However, while increasing the content of Sr with smaller ionic radii in $(Ba_{1-x}Sr_x)SnO_3$, the octahedral tilting distortion will take place in the corner-sharing octahedral network and the Sn-O-Sn bonds begin to bend increasingly, and finally form the orthorhombic perovskite crystal structure with Sn-O-Sn bond angle of about 160° in $SrSnO_3$ [27]. Accompanied with the Sn-O-Sn bond bending, the Sn 5s nonbonding characters of the conduction

band minimum recede and the antibonding character Sn 5*s*-O 2*p* contributions predominate gradually. As a result, the conduction band minimum was pushed up and the conduction band became narrower, while the band gaps increase correspondingly as shown in fig. 4(b). The increasing band gap trends resulted from the octahedral tilt effect are the same as that of other perovskite structured materials reported by Lee *et al.* [28]. However, the nonlinear variations in band gaps with composition were observed in $BaTi_{1-x}Zr_xO_3$ perovskite solid solutions [29,30]. The differences with our BSSO films may be due to the different effects of the A-site substitution and B-site substitution in the ABO_3 perovskites.

In conclusion, high-quality BSSO films with Sr content ranging from 0 to 1 were epitaxially grown on MgO substrates by pulsed laser deposition. X-ray diffraction, atomic force microscopy, and optical transmittance reveal that the Sr content affects the structural and optical properties of the BSSO films significantly. All films exhibit a high transparency of more than 90% in the visible and near-infrared range, and the root-mean-square surface roughnesses are strongly dependent on the Sr content. With increasing Sr content from 0 to 1 in the films, the lattice parameters decreased from 4.123 to 4.037 Å gradually, and the optical band gaps energy was found to increase from 3.50 to 4.27 eV linearly, which was attributed to the octahedral tilting distortion pushing up the minimum of the conduction band. The large structure and band gaps tuning suggest that the BSSO films have potential applications in the optoelectronic devices.

* * *

This work was supported by the Chinese Natural Science Foundation (No. 11004071).

REFERENCES

[1] Geske L., Lorenz V., Muller T., Jager L., Beige H., Abiche H. P. and Mueller V., *J. Eur. Ceram. Soc.*, **25** (2005) 2537.
[2] Lampe U., Gerblinger J. and Meixner H., *Sens. Actuators B: Chem.*, **26** (1995) 97.
[3] Tao S.W., Gao F., Liu X. Q. and Sørensen O. T., *Sens. Actuators B: Chem.*, **71** (2000) 223.
[4] Lampe U., Gerblinger J. and Meixner H., *Sens. Actuators B: Chem.*, **18** (1994) 132.
[5] Manorama S. V., Reddy C. V. G. and Rao V. J., *Appl. Surf. Sci.*, **174** (2001) 93.
[6] Wang H. F., Liu Q. Z., Chen F., Gao G. Y., Wu Wenbin and Chen X. H., *J. Appl. Phys.*, **101** (2007) 106105.
[7] Liu Q. Z., Wang H. F., Chen F. and Wu W, *J. Appl. Phys.*, **103** (2008) 093709.
[8] Liu Q. Z., Dai J. M., Liu Z. L., Zhang X. B., Zhu G. P. and Ding G. H., *J. Phys. D: Appl. Phys.*, **43** (2010) 455401.
[9] Balamurugan K., Harish kumar N., Ramachandran B., Ramachandra Rao M. S., Arout Chelvane J. and Santhosh P. N., *Solid State Commun.*, **149** (2009) 884.
[10] Balamurugan K., Harish Kimar N., Arout Chelvane J. and Santhosh P. N., *J. Alloys Compd.*, **472** (2009) 9.
[11] Yuan Y. P., Lv J., Jiang X. J., Li Z. S., Yu T., Zou Z. G. and Ye J. H., *Appl. Phys. Lett.*, **91** (2007) 094107.
[12] Borse P. H., Joshi U. A., Ji S. M., Jang J. S., Lee J. S., Jeong E. D. and Kim H. G., *Appl. Phys. Lett.*, **90** (2007) 034103.
[13] Endo T., Matsuda T., Takizana H. and Shimada M., *J. Mater. Sci. Lett.*, **11** (1992) 1330.
[14] Vegas A., Vallet-regi M., Gonzalez-calbet J. M. and Alario-rranco M. A., *Acta Cryst. B*, **42** (1986) 167.
[15] Cerda J., Arbiol J., Diaziaz R., Dezanneau G. and Morante J. R., *Mater. Lett.*, **56** (2002) 131.
[16] Smith A. J. and Welch A. J. E., *Acta Crystallogr.*, **13** (1960) 653.
[17] Chiba K., Makino S., Mukaida M., Kusunoki M. and Ohshima S., *Physica C*, **349** (2001) 35.
[18] Mukaida M., Miura M., Ichinose A., Matsumoto K., Yoshida Y., Horii S., Saito A., Hirose F., Takahashi Y. and Ohshima S., *Jpn. J. Appl. Phys.*, **44** (2005) 318.
[19] Mizoguchi H., Woodward P. M., Park C. and Keszler D. A., *J. Am. Chem. Soc.*, **126** (2004) 9796.
[20] Kumar A., Choudhary R. N. P., Singh B. P. and Thakur A. K., *Ceram. Int.*, **32** (2006) 73.
[21] Denton A. R. and Ashcroft N. W., *Phys. Rev. A*, **43** (1991) 3161.
[22] Srihari V., Sridharan V., Chandra S., Sastry V. S., Sahu H. K. and Sundar C. S., *J. Appl. Phys.*, **109** (2011) 013510.
[23] Shannon R. D. and Prewitt C. T., *Acta Crystallogr. Sect. B*, **25** (1969) 925.
[24] Ridha N. J., Yunus W. M. M., Halim S.A., Talib Z.A., Mohamad, Al-asfoor F. K. and Pimusr W. C., *Am. J. Eng. Appl. Sci.*, **2** (2009) 661.
[25] Tepehan F. Z., Ghodsi F. E., Ozer N. and Tepehan G. G., *Sol. Energy Mater. Sol. Cells*, **59** (1999) 265.
[26] Shimizu Y., Fukuyama Y., Narikiyo T., Arai H. and Seiyama T., *Chem. Lett.*, **14** (1985) 377.
[27] Mizoguchi H., Eng H. W. and Woodward P. M., *Inorg. Chem.*, **43** (2004) 1667.
[28] Lee S., Woodford W. H. and Randall C. A., *Appl. Phys. Lett.*, **92** (2008) 201909.
[29] Levin I., Cockayne E., Krayzman V., Woicik J. C., Lee S. and Randall C. A., *Phys. Rev. B*, **83** (2011) 094122.
[30] Lee S., Levi R. D., Quw G., Lee S. C. and Randall C. A., *J. Appl. Phys.*, **107** (2010) 023523.